Journal of Advanced Marine Engineering and Technology, Vol. 49, No. 3, pp. 206~214, 2025
J. Advanced Marine Engineering and Technology (JAMET)
https://doi.org/10.5916/jamet.2025.49.3.206

ISSN 2234-7925 (Print)
ISSN 2765-4796 (Online)
Original Paper

Simulation Study on a fuel cell/battery hybrid electric propulsion system for ships

San Kim[1] · Kyoung-Kuk Yoon[2] · Sang-Kyun Park†

(Received April 28, 2025 ; Revised June 1, 2025 ; Accepted June 23, 2025)

Abstract: This study focuses on modeling and simulating the components of a fuel cell/battery hybrid electric propulsion ship. The components were modeled and implemented in a simulation environment. Fuel cell systems can be broadly divided into three main subsystems: a polymer electrolyte membrane fuel cell (PEMFC) stack, fuel supply system, and a cooling system. The power system consists of a battery, converter and inverter units, an electric motor, and an energy management system (EMS) algorithm. To maintain system power balance, the EMS algorithm coordinates the fuel cell, battery, and load demands of the ship. In this study, a hybrid system combining a PEMFC and battery was developed by modeling each component and integrating them into a simulation environment. The simulation results confirmed that in the implemented system, the power demand generated by the operational profile, power produced by the fuel cell, and charging and discharging power of the battery were controlled to maintain balance.

Keywords: Polymer electrolyte fuel cell, Battery, Hybrid electric propulsion ship, Modeling, Simulation

1. Introduction

Owing to various environmental regulations **[1]**, research is being conducted to reduce pollutants and utilize ecofriendly propulsion systems **[2]**. Specifically, eco-friendly propulsion systems can eliminate pollutants completely, thereby preventing socioeconomic issues arising from environmental regulations. Among the researched eco-friendly propulsion systems, electric motors and eco-friendly engines are powered by alternative fuels, such as alcohol. Electric propulsion systems have been extensively applied in vehicles, with ongoing research and commercialization. However, the batteries used in electric propulsion systems have low-energy densities, resulting in short driving ranges and long charging times. To offset the drawbacks of electric propulsion, hybrid systems are occasionally developed by integrating engines with fuel cells **[3]**.

Fuel cells offer higher efficiency than engines and can store fuel in hydrogen tanks, thereby ensuring a longer operational range. However, owing to the relatively slow response of the system to external conditions, they can operate more effectively when integrated into a hybrid system with a battery. Hybrid systems using fuel cells and batteries have been implemented in various applications including 50 kW high-speed passenger vessels **[4]**, 30–40 kW submarine **[5]**, and modern Hyundai Nexo vehicles.

Owing to the difficulty in storing and handling hydrogen gas compared with petroleum-based fuels **[6]**, experimental data on fuel cells are relatively limited. However, simulation-based environments allow the efficient acquisition of virtual data related to system design parameters, performance prediction, cost analysis, and control algorithm testing. Because simulations are influenced by factors such as modeling fidelity, solver type, and initial parameters, validation based on comparisons with experimental data is necessary. Accordingly, for systems such as fuel cells that are difficult to handle experimentally, it is efficient to validate the simulation model using the available experimental data and conduct simulations under various conditions.

Simulation studies on fuel cell systems typically include research on the stack itself, auxiliary components such as the fuel supply and cooling systems, and the overall system. For example, studies on stacks investigated the fluid dynamics of heat exchange efficiency **[7]**, optimized channel design and operating conditions **[8]**, and improved efficiency based on the optimization of reactant gas management **[9]**. These studies consistently indicate that the temperature of the stack temperature has a major impact on chemical reaction rates and reactant behavior, both of which are directly linked to the overall system efficiency **[10]**.

Because gas supply is a critical factor affecting the

† Corresponding Author (ORCID: http://orcid.org/0000-0001-9981-6250): Professor, Division of Marine Information Technology, Korea Maritime & Ocean University, 727, Taejong-ro, Yeongdo-gu, Busan 49112, Korea, E-mail: skpark@kmou.ac.kr, Tel: 051-410-4579

1 Ph. D. Candidate, Division of Marine Engineering, Korea Maritime & Ocean University, E-mail: ks9524@g.kmou.ac.kr, Tel: 051-410-4579

2 Assistant Professor, Maritime AI and Cyber Security, Korea Maritime & Ocean University, E-mail: kkyoon@kmou.ac.kr, Tel:051-410-4265

performance and lifecycle of fuel cells, diverse studies have been conducted on fuel and air supply systems. Examples include the optimization of hydrogen delivery systems **[11]** and purge control strategies for air management **[12]**, both of which aimed at ensuring stable fuel cell operation. Building on previous studies, comprehensive research incorporating system-wide perspectives has explored energy management strategies that consider fuel-cell degradation **[13]** and fuel-cell modularization for large ships **[14]**.

Fuel cell systems in the maritime sector have been applied primarily to small-scale vessels, where air-cooled blower-based systems are commonly and extensively used owing to their simplicity and compactness **[15]**. However, these studies and applications are largely limited to low-capacity vessels, where the thermal load is relatively small and can be handled using simplified cooling systems. As the system capacity increases, particularly in medium-to-large-scale vessels, the thermal load increases substantially, necessitating more complex and robust thermal management strategies.

Therefore, this study proposes a simulation-based approach for analyzing a polymer electrolyte membrane fuel cell (PEMFC)/battery hybrid system with a two-stage liquid-cooling configuration, which is more suitable for high-capacity marine propulsion systems. Although these liquid-based cooling configurations have already been employed in large-scale facilities such as data centers **[16]** and commercial vessels, they have received limited academic attention, especially in the context of integrated hybrid fuel cell systems for maritime applications.

Accordingly, this study implements a simulation environment for a fuel cell/battery-powered ship incorporating a two-stage liquid cooling system, and investigates the thermodynamic behavior of the fuel cell stack under various system operating conditions. The research was conducted according to the following three-step process. First, a flowchart of the entire system was constructed to visualize the data flow between components, and key parameters were derived based on commercially available equipment specifications. Second, each component of the system was modeled using MATLAB Simulink. Third, a motor load profile was created based on the operational scenarios, and the output characteristics of the fuel cell/battery hybrid system were simulated and analyzed accordingly.

2. Design of the Fuel Cell/Battery Hybrid System

The fuel cell stack is typically more efficient than other propulsion systems, such as engines, but it is characterized by a relatively slow response time. Therefore, in mobility applications, such as vehicles and ships, hybrid systems that integrate fuel cells with batteries can be configured. As shown in **Figure 1**, a hybrid system can be configured by coupling a PEMFC with a battery.

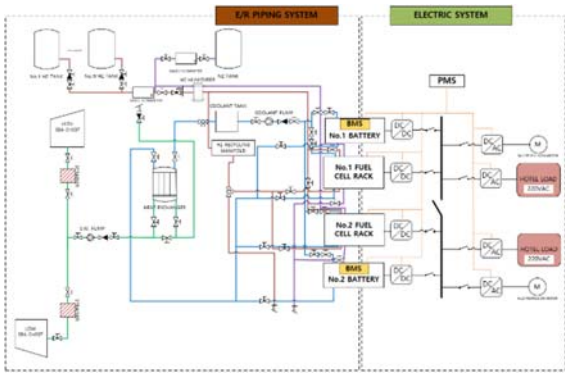

Figure 1: Model of the Fuel Cell/Battery Hybrid System

The left section of the figure shows the PEMFC system, which served as the main power source, along with the auxiliary equipment necessary for operation. The right section illustrates the power systems required to operate the batteries and motors. To operate the fuel cell stack, not only the stack itself but also a fuel supply system that provides hydrogen and oxygen, auxiliary equipment such as a coolant pump and seawater pump for stack cooling, and controllers, must be included. The power system consists of inverters, converters, motors, and batteries, all of which are required for the motor operation.

In a PEMFC/battery hybrid propulsion vessel, the total power load is the sum of the power consumed by the auxiliary equipment for fuel-cell operation and the power required by the motor and onboard loads. The energy management system (EMS) determines the load (A) of the fuel cell based on the current power demand. The battery is charged when the power produced by the fuel cell exceeds the power demand of the vessel. Conversely, when the power demand of the vessel is greater than the fuel cell output, the battery discharges to maintain power balance **[17]**.

3. Modeling of the Fuel Cell System

The voltage generated by the fuel cell stack can be expressed using **Equation (1) [18]**.

$$V_c = E_c - V_{act} - V_{\mathrm{ohm}} - V_{conc} \tag{1}$$

where V_c is the voltage of a single fuel cell, $E_c$is the open-circuit voltage, V_{act} is the activation voltage loss, V_{ohm} is the ohmic

resistance loss, V_{conc} is the concentration-loss voltage. The stack voltage can be expressed as the product of the single-cell voltage and number of cells, according to **Equation (2)**.

$$V_{stack} = n \times V_c \tag{2}$$

Multiplying by the current gives the power, as shown in **Equation (3)**. Additionally, the efficiency of the stack can be expressed by **Equation (4)**,

$$P_{stack} = n \times I \times V_c \tag{3}$$

$$n_{stack} = \frac{V_c}{1.25} \times 100 \tag{4}$$

The maximum mass of hydrogen that can react in a fuel cell is given by **Equation (5)**,

$$m_{H2,max} = \frac{M_{H2}}{2F} \times n \times I \tag{5}$$

Considering the hydrogen mass and power consumption of the two-phase cooling pumps and blowers, the overall system efficiency equation can be expressed using **Equation (6)**. In addition, the mass of hydrogen supplied to the stack should be less than or equal to the maximum hydrogen mass, as indicated by **Equation (7)**,

$$n_{system} = \frac{P_{stack} - P_{pump}}{m_{H2} \times 30356}, \tag{6}$$

$$m_{H2} < m_{H2,max} \tag{7}$$

The parameters of the fuel cell model used in this study are listed in **Table 1**. These parameters were simulated using various mathematical models and calculated as state variables of the system.

Table 1: Fuel cell specifications

Model	Calculation condition and unit	Data
PEMFC stack	Number of cells [-]	404
	Operating temperature of stack [K]	358
	Active cell area of one cell [cm^2]	380
Stoichiometric ratio	Fuel [-]	1.2
	Oxidant [-]	2
Humidity	Anode Inlet gas [%]	100
	Cathode Inlet gas [%]	100

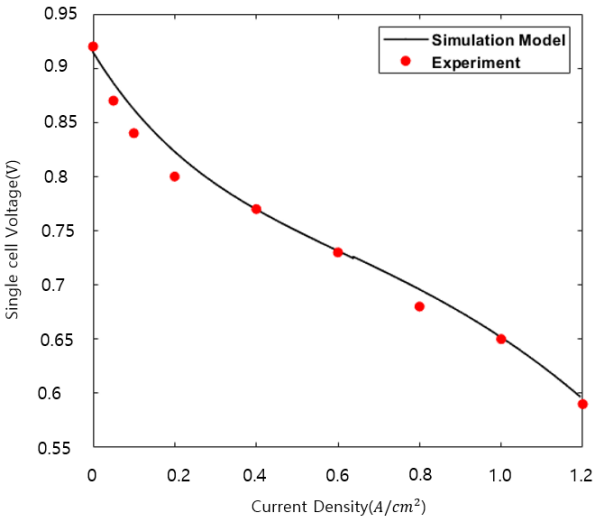

Figure 2: Comparison of stack's single-cell voltage between experiments and simulations

Figure 2 presents the simulation and experimental results for the single-cell voltage of the fuel cell stack. The simulation was performed by gradually increasing the current density after the stack temperature reached 70°C.

The simulated and experimental voltages of the fuel cell stack exhibited a maximum deviation of 0.02 V, which corresponded to an error of 5%. Furthermore, a comparison of the simulated and experimental data confirms that both exhibit similar trends.

4. Simulation of the PEMFC/Battery Hybrid System

The hybrid power system, including the fuel cell stack, can be configured as shown in **Figure 3**.

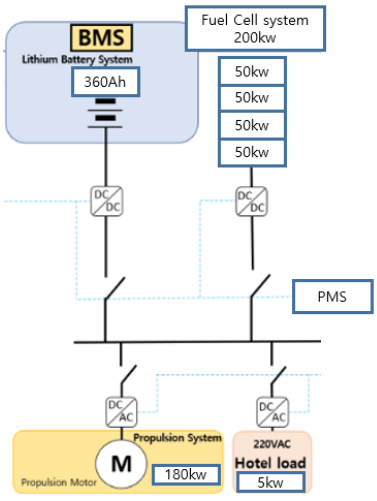

Figure 3: Power System Configuration

Table 2: Hybrid system specifications

Model	Calculation condition and unit	Data
PEMFC stack	Power[kW]	180
	Voltage[V]	140-260
	Reference Temperature[K]	338
Battery	Capacity[Ah]	360
	Voltage[V]	560
	Initial SOC[%]	60
Motor Peak Power	Power[kW]	200
DC-Grid	Voltage[V]	1500

The system consists of a PEMFC rack composed of four 50 kW fuel cell stacks, a battery, direct current (DC)–DC converters, DC–alternating current inverters, and a motor system. When a propulsion signal is generated or an internal load occurs, the power demand fluctuates and is managed by the fuel cell system and battery. **Table 2** lists the specifications of the power system used in the study.

When all power devices achieve balance within the system, the power equation can be expressed as follows:

$$P_{Pemfc} + P_{Bat}^{+} = P_{Motor} + P_{Aux} + P_{Bat}^{-} \tag{8}$$

where P_{Pemfc} represents the power generated by the fuel cell, P_{Bat}^{+} represents the power discharged by the battery, P_{Bat}^{-} represents the power used to charge the battery, P_{Motor} represents the power required to drive the motor according to user demand, and P_{Aux} represents the power required for the auxiliary equipment and internal systems of the vessel. The open-circuit voltage during the discharging and charging processes of a battery can be represented by the following equations **[19]**:

Charging mode:

$$E_{Bat_{Dis}} = E_0 - K\frac{Q_{max}}{Q_{max} - Q_t}i^* - K\frac{Q_{max}}{Q_{max} - Q_t}Q_t + Aexp(-BQ_t) \tag{9}$$

Discharging mode:

$$E_{Bat_{Chg}} = E_0 - K\frac{Q_{max}}{0.1Q_{max} - Q_t}i^* - K\frac{Q_{max}}{Q_{max} - Q_t}Q_t + Aexp(-BQ_t) \tag{10}$$

where $E_{Bat,Dis}$ and $E_{Bat,Chg}$ represent the open-circuit voltage during battery discharge and charging, respectively, E_0 denotes the constant voltage of the battery, K is the polarization constant, i^* refers to the low-frequency current dynamics, Q_t is the current charge of the battery, A is the exponential coefficient for the battery voltage, and B is the exponential coefficient for the battery capacity. The state of charge (SOC) of the battery at a specific time can be defined according to **Equation (11) [20]**:

$$SOC_t = SOC_0(0) - \frac{Q_t}{C_t}\eta_c \tag{11}$$

where SOC_0 represents the initial state of charge of the battery, C_t is the battery capacity, and η_c is the efficiency constant of the battery.

The battery used in this study is a lithium battery, which is the most efficient when operating within an SOC range of 50–80%. In addition, during rapid changes in the system, the battery was charged or discharged to handle the peak power. However, it should be controlled to ensure that the current does not exceed the maximum value specified by the manufacturer.

Furthermore, this study investigated the dynamic behavior of a hybrid fuel cell/battery system in the time domain using a Simulink-based model. The simulation was conducted continuously with a fixed step size of 0.001 s over a total simulation period of 30'0 s. The primary input variables were defined based on the motor's speed and load demand according to the operational scenarios, and the analysis encompassed system-wide energy flow, control responses, and thermal characteristics.

5. Analysis of Simulation Results

Figure 4 shows the motor's rotational speed configuration (in RPM) used for the simulation of the 200 kW hybrid ship, designed to generate data under various load conditions for the fuel cell/battery hybrid ship system. The RPM work profile represents the control signals derived from the user operations, which are converted into motor RPM commands. The maximum and minimum RPM values were determined based on the motor's specifications, and the resulting profile was used as the primary input for the simulation. The simulation environment was designed to output the state variables of each subsystem in response to the dynamically changing RPM inputs.

Figure 5 shows the power variations in the fuel-cell/battery hybrid system in response to the defined motor's speed and onboard load. Specifically, fuel cell power (in blue) indicates the power generated by the fuel cell system, whereas motor and

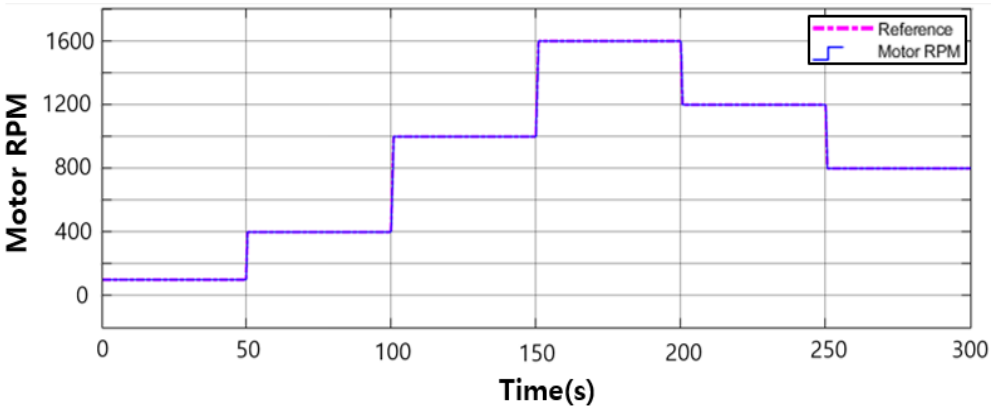

Figure 4: Plot of Motor's Rotational Speed (Revolutions Per Minute (RPM)) as a Function of time (Work Profile)

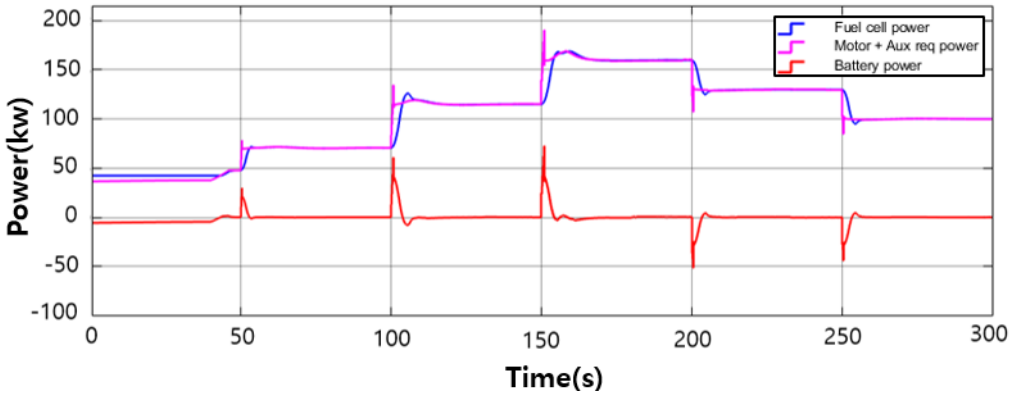

Figure 5: Analysis of Fuel Cell System Power Data

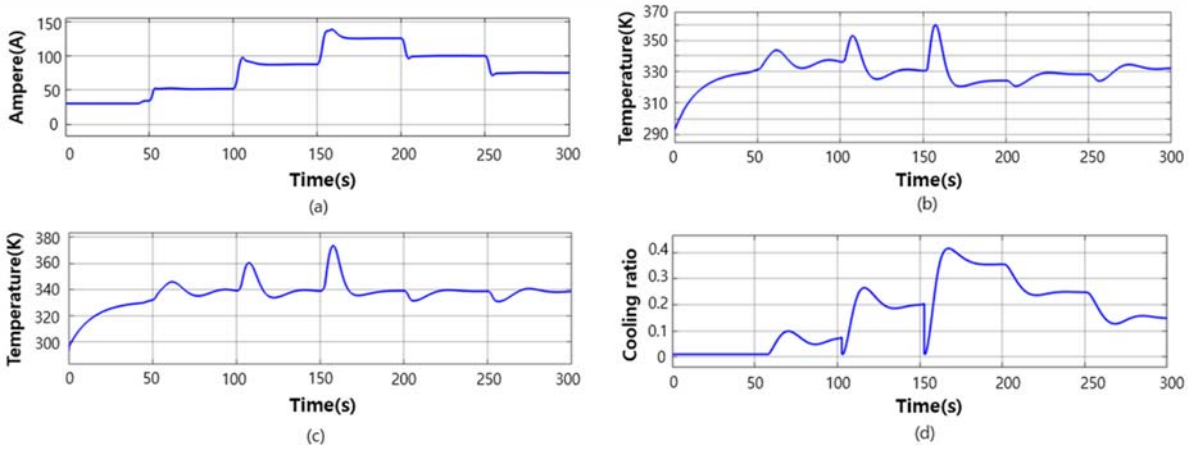

Figure 6: Analysis of Fuel Cell System Equipment Data

(a: Stack load, b: Coolant temperature, c: Stack temperature, d: Coolant heat exchange ratio)

auxiliary power (in magenta) refers to the combined power required for motor operation, according to the given RPM profile and consumption by auxiliary systems. The battery power (in red) denotes the contribution of the battery, exhibiting negative and positive values during charging and discharging, respectively.

Before the 50-s mark in the simulation, the fuel cell output exceeded the required power. This indicates that the required power is lower than the minimum power output of the fuel cell, and that the battery power becomes negative, indicating that the battery is being charged. Hence, before 50 s, both the motor and onboard loads required less power than the minimum generated by the

fuel cell, and the excess energy was used to charge the battery.

In the proximity of the 50-s mark, the required power for the motor also increased as the motor RPM increased, reaching the minimum power output of the fuel cell. The battery power began to converge from the negative region toward zero, indicating that as the motor load increased, the charging rate of the battery decreased.

The motor power demand, shown in magenta color in **Figure 5**, exhibits a trend similar to that of the motor's speed (in RPM) in **Figure 4**, even though the motor's speed yields a stepped pattern without fluctuations, whereas the corresponding power output yields overshoot and undershoot responses. This discrepancy is due to the control delays caused by the switching actions and the inertia of the motor shaft.

In the 100–200 s range, the motor's demand and battery powers continued to display similar trends to those observed at 50 s. However, as the motor RPM increased, the overshoot in the motor power became more pronounced at each step, and the maximum discharge power of the battery increased. Upon reaching the 200-s mark, the motor's speed started to decrease, and the motor's demand power yielded an undershoot response in the opposite direction compared with that in the 50–150-s interval. Once the motor's speed stabilized, the motor power demand eventually leveled off after a short period, a phenomenon attributed to system inertia and control delays, similar to the response attained when the motor's speed increased.

During the 200–300 s interval, the motor's demand power and battery power continued to exhibit patterns similar to those observed during the 150–200 s interval. However, as the motor's speed decreased, the intensity of the undershoot of the motor's power became less pronounced. Battery charging occurred when the fuel-cell power exceeded the motor demand at 200 s and 250 s, and the undershoot at 200 s was greater than that at 250 s.

Figure 6 shows the detailed responses of the fuel cell system subject to variations in motor's speed. The load on the fuel cell stack (a) was determined by the power management system, which adjusted the cell's current to match the required power demand. In this simulation, the load was proportionally increased or decreased according to the power demand, resulting in a pattern that closely followed the motor load profile.

The state variables of the cooling system in response to the fuel cell load included the (b) inlet temperature of the coolant entering the stack, (c) temperature of the fuel cell stack, and (d) the cooling ratio, which corresponded to the opening rate of the 3-way valve that directed the coolant flow toward the heat exchanger. Specifically, the coolant inlet temperature shown in **Figure 6**(b) varied significantly depending on the load conditions. During the low-load phase (50–100 s), the coolant entered the stack at a relatively high temperature of approximately 330–350 K. As the load increased (at approximately 150 s), the inlet temperature decreased to approximately 325–330 K. During the highest load period (150–200 s), it reached a minimum range of approximately 325–328 K. After the load decreased (200–300 s), the coolant temperature increased again to 320–330 K and 325–330 K. This pattern reflects thermal regulation toward the target control temperature of the stack; when subjected to a low load, the warmer coolant helps raise the stack temperature, whereas when subjected to a high load, the cooler coolant enhances heat removal. These observations indicate that the coolant inlet temperature is actively controlled to maintain the fuel cell operation within its optimal efficiency range.

As shown in **Figure 6**(c), when the stack load increases or decreases, the stack temperature momentarily deviates from the control set point (338 K) but rapidly converges within approximately 30 s, confirming the responsiveness of the thermal control system.

The cooling ratio shown in **Figure 6**(d) represents the proportion of coolant heated by the fuel cell stack directed to the heat exchanger, and is determined by a 3-way valve controlled by a proportional integral (PI) controller. The actuation speed of the valve reflects the temperature-tracking responsiveness of the cooling system, whereas the degree of convergence of its value indicates the thermal stability. At the time of maximum load (approximately 150 s), the cooling ratio approached 0.4, suggesting that the system was designed to accommodate significant thermal loads with an appropriate safety factor.

Therefore, by evaluating the temperature tracking speed and thermal stability of the system, it is possible to back-calculate design parameters such as the PI controller gains, maximum mass flow rates of the coolant and seawater pumps, and effective heat transfer area of the heat exchanger. These parameters can then be adjusted according to a predefined safety factor to guide the system design.

Figure 7 shows the changes in the battery's SOC and current during the same simulation. The current was defined as positive during discharging and negative during charging.

The SOC increased as the excess power generated by the fuel cell was used to charge the battery because the motor power demand at the initial RPM was smaller than the fuel cell output. As

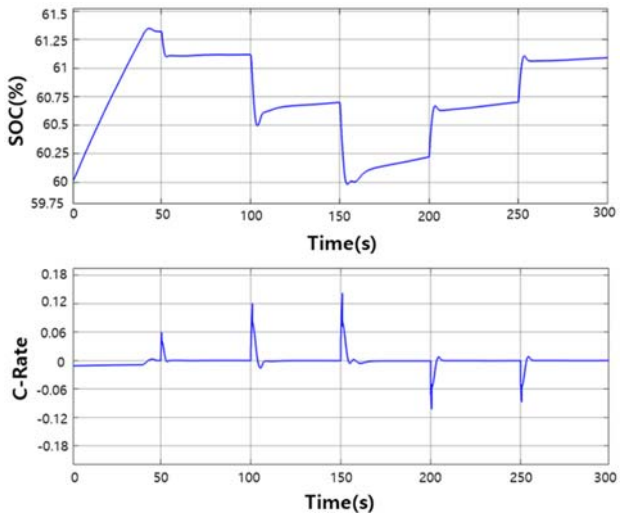

Figure 7: Battery Variation According to Operating Conditions (SOC, Current)

the simulation time approached 50 s, the power generated by the fuel cell balanced the motor power demand and the SOC stabilized at a certain level. After 50 s, an overshoot occurred that temporarily accelerated the motor as the motor load increased, causing the battery to discharge and the SOC to decrease. Once the fuel cell load reached the motor power demand, the battery discharging process ended and the SOC remained stable.

From 100 s onward, the system underwent a similar discharge and stabilization process as the motor load increased, as observed at 50 s. Additionally, as the motor load increased, the intensity of the peak power during the control interval also increased, leading to an amplified control signal in which the fuel cell power momentarily exceeded the motor load. Between 100 and 150 s, the fuel cell load was adjusted by the PI controller. During this time, the battery was charged, slightly increasing the SOC. A similar process occurred from 150 s to 200 s, with excess power from the fuel cell charging the battery and maintaining the system's power balance while the fuel cell power converged.

After 200 s, the motor load decreased. When the target load was reached, temporary deceleration occurred, and the power values experienced an undershoot, opposite to the behavior observed between 50 and 150 s, generating excess fuel cell power. To maintain the balance between the fuel cell excess and the required power, the battery was briefly charged, leading to a temporary increase in the SOC at approximately 200 s and 250 s. As the fuel cell system stabilized, the SOC value became more stable manifested by a gradual charging process.

Comparison of the slopes of the SOC values during periods of low SOC (150–200 s) and high SOC (50–100 s, 250–300 s) shows that as the SOC increases, the slope of the graph decreases. This indicates that the system controls the charging intensity according to the charge level of the battery to maintain a specific SOC range.

The current values of the battery show that during the overshoot power occurrence at 50, 100, and 150 s, the battery discharges and currents are positive. At 200 and 250 s, when an undershoot occurs, the battery charges and the current becomes negative. Considering the battery specifications, this corresponds to a maximum C-rate of approximately 0.14, which is lower than that specified by the manufacturer.

Consequently, the simulation can be used to evaluate the hydrogen consumption of the fuel cell and the corresponding SOC variation in the battery for a given operational profile. This enables the estimation of design parameters such as battery capacity and DC/DC converter duty ratio, considering the ship's operational profile and mission duration. Furthermore, because the simulator allows for a flexible configuration of work profiles and system specifications, it can be applied to economic assessments, optimization studies, and evaluation of various EMS control strategies.

6. Conclusion

The objective of this study was to implement a simulation environment for a hybrid fuel cell/battery propulsion system for ships. The results of this study can be summarized as follows:

① A 200 kW PEMFC was modeled, and single-voltage data were compared and validated using experimental data. In addition, the power system components, including the fuel cell system, battery, and motor were modeled, and a simulation environment was established by integrating these components.

② It was observed that when the temperature of the fuel cell stack was lower than the control temperature, the valve was controlled to increase the temperature of the stack so that the heat generation exceeded the cooling rate. Conversely, when the stack temperature was higher than the control temperature, the valve was controlled to decrease the stack temperature by ensuring that the heat generation was less than the cooling rate. This demonstrated that the cooling system of the fuel cell stack was regulated to maintain the control temperature of the stack.

③ The hybrid fuel cell/battery system implemented in this study operated the fuel cell continuously while charging and discharging the battery (which had a fast response time) to maintain the power balance during instantaneous power fluctuations.

④ In the simulation, the time required for the system to stabilize due to variations in the motor's speed was much smaller than the actual load fluctuation period of the ship. Therefore, it was confirmed that the hybrid fuel cell/battery system was designed to achieve fast responses and could stably track specific load conditions.

As a result, the proposed simulation environment enables the extraction of design parameters, such as PI controller gains, pump flow rates, and heat exchanger area, as well as battery sizing and converter configurations based on operational profiles. Additionally, the flexibility of the simulator allows its application in economic evaluations, system optimization studies, and EMS strategy testing, providing a practical foundation for real-world marine hybrid propulsion design.

Acknowledgement

This research was supported by the technology innovation program (No. 00144016) funded by the Ministry of Trade, Industry & Energy (MOTIE, Korea).

Author Contributions

Conceptualization, S. Kim and S. K. Park; Methodology, S. Kim and S. K. Park; Software, S. Kim and S. K. Park; Validation, S. Kim and S. K. Park; Formal Analysis, S. K. Park; Investigation, S. Kim; Resources, All Author; Data Curation, S. Kim; Writing—Original Draft Preparation, S. Kim and S. K. Park; Writing—Review & Editing, S. K. Park; Visualization, S. Kim; Supervision, S. K. Park; Project Administration, S. K. Park and K.K Yoon; Funding Acquisition, S. K. Park and K.K Yoon.

References

[1] American Bureau of Shipping (ABS), MEPC 72 Brief, https://ww2.eagle.org/content/dam/eagle/regulatory-news/2018/MEPC%2072%20Brief%20FINAL.pdf, Accessed August 8 2020.

[2] A. B. Stambouli, "Fuel cells: The expectations for an environmental-friendly and sustainable source of energy," Renewable and Sustainable Energy Reviews, vol. 15, no. 9, pp. 4507-4520, 2011.

[3] Z. Jiang, L. Gao, M. J. Blackwelder, and R. A. Dougal, "Design and experimental tests of control strategies for active hybrid fuel cell/battery power sources," Journal of Power Sources, vol. 130, pp. 163–170, 2004.

[4] J. W. Prattand and L. E. Klebanoff, Feasibility of the SFBREEZE: aZero-Emission, Hydrogen Fuel Cell, High Speed Passenger Ferry, SANDIA REPORT, SAND 2016-9719, pp. 48-51, 2016.

[5] K. Strasser, H2/O2-PEM-fuel Cell Module for an Air Independent Propulsion System in a Submarine, John Wiley & Sons, 2010.

[6] X. Mao, R. Ying, Y. Yuan, F. Li, and B. Shen, "Simulation and analysis of hydrogen leakage and explosion behaviors in various compartments on a hydrogen fuel cell ship," International Journal of Hydrogen Energy, vol. 46, no. 9, pp. 6857-6862, 2021.

[7] M. Ghasabehi, M. Ashrafi, and M. Shams, "Performance analysis of an innovative parallel flow field design of proton exchange membrane fuel cells using multiphysics simulation," Fuel, vol. 285, 119194, 2021.

[8] Z. Liu, X. Zeng, Y. Ge, J. Shen, and W. Liu, "Multi-objective optimization of operating conditions and channel structure for a proton exchange membrane fuel cell," International Journal of Heat and Mass Transfer, vol. 111, pp. 289-298, 2017.

[9] O. S. Ijaodola, Z. El-Hassan, E. Ogungbemi, F. N. Khatib, T. Wilberforce, J. Thompson, and A. G. Olabi, "Energy efficiency improvements by investigating the water flooding management on proton exchange membrane fuel cell (PEMFC)," Energy, vol. 179, pp. 248-251, 2019.

[10] J. -W. Ahn and S. -Y. Choe, "Coolant controls of a PEM fuel cell system," Journal of Power Sources, vol. 179, no. 1, pp. 260-263, Energy, vol. 179, pp. 252-264, 2008.

[11] H. Chen, Z. Liu, X. Ye, L. Yi, S. Xu, and T. Zhang, "Air flow and pressure optimization for air supply in proton exchange membrane fuel cell system," Energy, vol. 238, 121949, 2022.

[12] D. Yang, R. Pan, Y. Wang, and Z. Chen, "Modeling and control of PEMFC air supply system based on T-S fuzzy theory and predictive control," Energy, vol. 188, 116078, 2019.

[13] D. Pivetta, C. Dall'Armi, and R. Taccani, "Multi-objective optimization of hybrid PEMFC/Li-ion battery propulsion systems for small and medium size ferries," International

Journal of Hydrogen Energy, vol. 46, no. 72, pp. 35953-35958, 2021.

[14] E. S. Bang, Y. -M. Kim, M. -H. Kim, and S. -K. Park, "Development of a 240 kW PEMFC system model for a ship," Journal of Advanced Marine Engineering and Technology, vol. 44, no. 4, pp. 274-281, 2020.

[15] J. Han, J. Han, H. Ji, and S. Yu, ""Model-based" design of thermal management system of a fuel cell "air-independent " propulsion system for underwater shipboard," International Journal of Hydrogen Energy, vol. 45, no. 56, pp. 32457-32461, 2020.

[16] A. Carbó, E. Oró, J. Salom, M. Canuto, M. Macías, and J. Guitart, "Experimental and numerical analysis for potential heat reuse in liquid cooled data centers," Energy Conversion and Management, vol. 112, pp. 138–142, 2016.

[17] J. Han, J. Charpentier, and T. Tang, "An energy management system of a fuel cell/battery hybrid boat," Energies, vol. 7, no. 5, pp. 2801-2808, 2014.

[18] J. T. Pukrushpan, Modeling and Control of Fuel Cell Systems and Fuel Processors, Ph. D. Dissertation, Mechanical Engineering, University of Michigan, USA, 2003.

[19] Z. ZHANG, C. GUAN, and Z. LIU, "Real-time optimization energy management strategy for fuel cell hybrid ships considering power sources degradation," IEEE, vol. 8, pp. 87048-87054, 2020.

[20] O. Tremblay, L. -A. Dessaint, and A. -I. Dekkiche, "A generic battery model for the dynamic simulation of hybrid electric vehicles", IEEE, vol. 8, pp. 87048-87054, 2020.